Phase behavior of a Carbon dioxide/Toluene/Polymethyl methacrylate ternary system

Takumi Tachibana[1], Hiroaki Matsukawa[2], Yuya Murakami[2], Atsushi Shono[2], and Katsuto Otake[2]*

[1] Department of Industrial Chemistry, Graduate School of Engineering, Tokyo University of Science, 12-1 Ichigayafunagawara-machi, Shinjuku-ku, Tokyo 162-0826, Japan
[2] Department of Industrial Chemistry, Faculty of Engineering, Tokyo University of Science, 12-1 Ichigayafunagawara-machi, Shinjuku-ku, Tokyo 162-0826, Japan

* To whom correspondence should be addressed.
E-mail : k-otake@ci.kagu.tus.ac.jp Tel : +81-3-5228-8052

Abstract

The Phase behavior of a carbon dioxide (CO_2)/toluene (Tol)/poly(methylmethacrylate) (PMMA) ternary system was measured. The measurements were performed using a synthetic method combined with a laser displacement and a reflected light intensity measurement. The bubble points (vapor-liquid phase separation) were determined from the change in the displacement of the piston, and the cloud points (liquid-liquid phase separation) were determined from the change in the reflected light intensity. The phase boundaries of CO_2 mass fractions ranging from 0.098 to 0.475 with varying the Tol/PMMA ratio were measured. The homogeneous phase area decreased when the ratio of PMMA to Tol increased and/or the temperature decreased. The liquid-liquid (LL) line of a CO_2/Tol/PMMA ternary system separates from the vapor-liquid (VL) line at a higher CO_2 mass fraction compared to poly(styrene) previously reported, and it shows more less CO_2 mass fraction dependence. These changes in the LL phase separation behavior were explained with the free volume and solubility parameter estimated using the Sanchez-Lacombe equation of state.

Keywords

Vapor-liquid equilibrium; Liquid-liquid equilibrium; Vapor-liquid-liquid equilibrium; Carbon dioxide; Toluene; Polymethyl methacrylate; Synthetic method; Laser turbidimetry; Laser rangefinder; Sanchez-Lacombe Equation of State

1. *Introduction*

Supercritical carbon dioxide ($scCO_2$) has many advantages, such as low cost, non-toxicity, non-flammability, and chemical inertness; moreover, its physicochemical properties can be tuned by pressure and/or temperature variation. The combination of CO_2/organic solvent/polymer appears in a variety of processes. One example is the supercritical polymerization process. In this process, $scCO_2$ is used as a reaction solvent and has various advantages. For example, the use of the CO_2 reduces and/or removes the use of harmful organic solvents from the process. Furthermore, since CO_2 is a gas at atmospheric pressure, it can be easily separated from the polymer by simply reducing the pressure of CO_2 to atmospheric pressure, thus the solvent removal process could be eliminated. DeSimone *et al.* [1] and Canelas *et al.* [2] reported the dispersion polymerization of a poly(methylmethacrylate) (PMMA) and a poly(styrene) (PS) in $scCO_2$, respectively. In both polymerizations, together with the use of specially designed surfactant, the polymers were obtained in high yields and with micrometer-sized particles with narrow size distributions. Recently, Bassert *et al.* [3] investigated the stereoselective, solvent-free ring-opening polymerization of lactide in $scCO_2$, and reported that the reaction temperature could be lowered to reduce the energy requirement compared to conventional methods. For these three cases, as unreacted residual monomers dissolve in CO_2, it can be removed form the polymer by washing with high pressure CO_2. For the removal of solvents and monomers, understanding of the phase behavior of CO_2/monomer/polymer ternary systems are important.

Another example is the particulate process with $scCO_2$. There are several types of particulate processes with $scCO_2$. In particular, the anti-solvent method, such as the gas anti-solvent method and the supercritical fluid anti-solvent method, involves blowing $scCO_2$ into an organic solvent solution of the target material to reduce the solubility of the material to precipitate the solute. Dixon *et al.* [4] have succeeded in forming polymer particles with a diameter of 0.1~20 μm by spraying polystyrene (PS)/toluene (Tol) mixtures into $scCO_2$ from a capillary; this method is the gas anti-solvent method. Prosapio *et al.* [5] reported that polyvinyl alcohol particles with a smooth surface of 2-9 μm were obtained using ethanol, acetone, and isopropanol as co-solvent by the gas anti-solvent method. In recent years, there have been studies on the formation of biocompatible polymer-drug composite particles formation for drug delivery with $scCO_2$. Franco *et al.* [6] reported the formation of polyvinylpyrrolidone and ketoprofen composite particles using dimethyl sulfoxide as a co-solvent. An increase in the drug dissolution rate in the particles of about 4 times with respect to the unprocessed ketoprofen was observed. When $scCO_2$, which is a poor solvent for the polymer, is added to the polymer solution, the solvency of the solvent decreases to induce phase separation of polymer solution. Understanding of the phase behavior of CO_2/solvent/polymer ternary systems are also

important in such processes.

Other attempts to add organic solvents in the preparation of polymeric foams using $scCO_2$ as the blowing agent have been reported [7], and it is said that liquid-liquid (LL) phase separation is one factor that affects the bubble diameter of the foam. Therefore, the phase behavior of the CO_2/organic solvent/polymer ternary system is essential for the design of these processes. Most of the phase equilibria of CO_2/organic solvent /polymer ternary systems are described using *PT* phase diagrams. These phase diagrams are classified into UCST type, LCST type, and U-LCST type phase behavior according to the behavior of LL phase separation with respect to temperature [8]. And it is known that phase behavior varies with parameters such as composition and molecular weight of the polymer. In order to gather information necessary for the supercritical polymerization process, Byun *et al.* [9-12] reported the phase behavior of ternary systems of CO_2, a variety of poly(alkyl acrylates), and their monomers. They reported that the phase behavior changes depending on the alkyl chain of the polymer. Hasch *et al.* [13] reported the phase diagram of a CO_2/acetone/polyethylene ternary system and found that as the acetone concentration increased, the system changed from exhibiting UCST-type behavior to U-LCST-type and LCST-type behaviors. They explained the phase behavior from the context of the polyethylene precipitation due to an increase in acetone-acetone interaction as the acetone concentration increased. Campardelli *et al.* [14] and Santos *et al.* [15] reported the *Px* phase diagram of CO_2/organic solvent/polymer ternary systems. Kim *et al.* [10, 16, 17] also reported on the *Px* phase diagram in part. We reported the *Px* phase diagram of CO_2/silicon alkoxide/polymer and CO_2/toluene/PS ternary systems [18-20]. The LL phase boundary behavior with respect to concentration at constant temperature can be ascertained from *Px* diagrams. We reported that the phase behavior varies with parameters such as concentration, temperature, and molecular weight of the polymer. In addition, we discussed the differences in phase behavior depending on the solvent and polymer species. Unfortunately, there are fewer reported *Px* diagrams compared to *PT* phase diagrams, which do not provide sufficient information.

In this work, to deepen the knowledge of the phase behavior of CO_2/organic solvent/polymer systems, the phase behavior of a CO_2/Toluene/PMMA ternary system was measured over a wide range of temperature, pressure, and polymer mass fraction using a synthetic method combined with a laser rangefinder and a laser turbidimetry. The effect of individual parameters on the phase behavior has often been explained by the free volume (FV) difference between the components [8, 9]. Furthermore, we have explained the effect of solvent and polymer species by solubility parameters (SP) [18, 19]. It is known that the FV and SP can be obtained using the equation of state (EoS) [21-24]. In this work, the FV and SP of pure components and CO_2/Tol mixtures were estimated using the Sanchez-Lacombe (SL) EoS [25-27], and the effects of individual parameters, such as composition, temperature, and polymer

specie, for the phase diagrams were discussed.

2. Experimental

2.1. Materials

Carbon dioxide (CO_2, CAS number [124-38-9], purity >99.99%) was purchased from Fujii Bussan Co. Toluene (Tol, CAS number [108-88-3], purity >99.5%) was purchased from Kanto Kagaku Co. Poly(methylmethacrylate) (PMMA, CAS number [9011-14-7], Mw = 35,000, Mw/Mn = 1.871) was purchased from Across Organics Co. All the materials were used as received. The specifications of pure CO_2, Tol, and PMMA are listed in Table 1.

Table 1. Specifications of pure components.

Component	CAS number	Supplier	Mole fraction purity (Supplier)	
Carbon dioxide, CO_2	124-38-9	Fujii Bussan Co.		0.9999
Toluene, Tol	108-88-3	Kanto Kagaku Co.		0.995
Poly(methyl methacrylate), PMMA	9011-14-7	Across Oraganics Co.	M_w	35,000
			M_w/M_n	1.871

2.2. Apparatus and Procedure

In this work, the ternary system phase diagram was deduced using a synthetic method. In this system, the vapor-liquid (VL) and vapor-liquid-liquid (VLL) phase separation (bubble points, BP) and the LL phase separation (cloud points, CP) were observed as the phase separation points. The BP were measured by the method combined with a laser rangefinder, and the CP was measure by the method combined with a laser turbidimetry. The details of the experimental apparatus and procedures employed have been described elsewhere[20, 28].

In brief, appropriate amounts of PMMA, Tol, and CO_2 were introduced into the front part of a variable-volume view cell containing a moving piston. The composition in the front part of the cell was calculated from the mass of the materials. The cell was heated to the desired temperature and then pressurized by moving the piston from the back part of the cell until a single phase was achieved. Next, the pressure was slowly decreased while measuring turbidity and piston displacement. The BP is defined as the point at which vapor phase separation occurs, and determined from the relationship of pressure and displacement of the piston. The CP is defined as the point at which the turbidity changes due to the formation of second liquid phase.

2.3. Estimation using SL EoS

2.3.1. SL EoS

SL EoS [25-27] is mainly used to study polymeric solutions and is applicable to large-molecule systems such as macromolecules because it does not require a critical value as a pure component parameter. The accuracy of density estimation is also important to estimate the free volume and solubility parameters. We discussed the estimation accuracy of the density of CO_2/Tol homogeneous mixtures using three EoSs in the previous work [29], and found that SL EoS showed good estimation accuracy. In this work, the SL EoS was used for the estimation of the free volume and the solubility parameter. The SL EoS is expressed as follows

$$\tilde{\rho}^2 + \tilde{P} + \tilde{T}\left\{\ln\left(1-\tilde{\rho}\right) + \left(1-1/r\right)\tilde{\rho}\right\} = 0$$

$$\tilde{T} = T/T^*, \quad \tilde{P} = P/P^*, \quad \tilde{\rho} = \rho/\rho^* = V^*/V \tag{1}$$

where T, P, and ρ are the temperature, pressure, and density, respectively. $\tilde{T}$, $\tilde{P}$, and $\tilde{\rho}$ represent the reduced parameters; T^*, P^*, and ρ^* are characteristic parameters of the pure component; R is the gas constant; and r is the number of segments. In order to calculate the mixture using the EoS, it is necessary to apply the mixing rule. The original mixing rule reported by Sanchez *et al*. [30] is expressed as follows;

$$\frac{1}{V^*} = \sum_i \frac{\phi_i}{V_i^*} \tag{2}$$

$$\phi_i = \frac{w_i/\rho_i^*}{\sum_j w_j/\rho_j^*} \tag{3}$$

$$P^* = \sum_i \phi_i P_i^* - RT\sum_j \sum_{i<j} \phi_i \phi_j \chi_{ij} \tag{4}$$

$$\chi_{ij} = \frac{P_i^* + P_j^* - 2\left(1-k_{ij}\right)\left(P_i^* P_j^*\right)^{1/2}}{RT} \tag{5}$$

$$T^* = \frac{P^* v_0}{R} \tag{6}$$

$$\frac{1}{v_0} = \sum_i \phi_i \left(\frac{P_i^*}{RT_i^*}\right) \tag{7}$$

where v_0 is the volume of a lattice site. ϕ_i and w_i are the close-packed volume fraction and mass fraction of the i^{th} component, respectively. χ_{ij} is the *i-j* interaction term, and k_{ij} is the *i-j* interaction parameter. The interaction parameter k_{ij} is obtained by correlating the thermodynamic properties of the mixture. In this work, the interaction parameter between CO_2

and Tol was obtained by correlating the density of CO_2/Tol homogeneous mixture [29]. The pure component parameters and interaction parameter used in this study are summarized in Table 2 [26, 27, 30].

Table 2. SL characteristic parameters for pure substances used in the SL EoS.

Component	P^* / MPa	T^* / K	ρ^* / kg m^{-3}
CO_2	574.5[a]	305[a]	1510[a]
Tol	397[b]	543[b]	966[b]
PMMA	696[b]	503[b]	1269[b]

[a] Reported by Kiran *et al.* [30]

[b] Reported by Sanchez *et al*. [26, 27]

2.3.2. Free volume

In SL EoS, a molecule is a collection of segments, and the volume of substance is represented by the occupied volume of the molecule and the vacancies. The volume of these vacancies can be regarded as the FV of the molecule. The characteristic parameters T^*, P^*, and ρ^* of the SL EoS can be used to obtain the lattice parameters r, ε^*, and v^* of the pure components based on the lattice fluid theory, as follows:

$$r = P^* V^* / RT^* \tag{8}$$

$$\varepsilon^* = RT^* \tag{9}$$

$$v^* = RT^* / P^* \tag{10}$$

where ε^* is the interaction energy between segments, and v^* is the lattice volume, which is also indicative of segment volume forming molecular. Then, the occupied volume v_0 of the molecule can be obtained as follows

$$v_0 = rv^* \tag{11}$$

The FV v_f can then be obtained by subtracting the occupied volume from the volume as follows [24]:

$$v_f = V - v_0 \tag{12}$$

2.3.3. Solubility parameter

SP is a physical property which can be used as an indicator of solubility, affinity, oil resistance, and water resistance of organic materials. Nowadays, it is often applied to organic materials, especially polymers. The SP σ is related to the cohesive energy density (CED), which is defined as the internal energy (ΔU) per unit volume [31]:

$$\sigma^2 = CED = \frac{\Delta U}{V} = \frac{\Delta H_v - RT}{V} \tag{13}$$

where ΔH_v is the enthalpy of vaporization. To obtain the SP, the heat of vaporization of a substance to be calculated. Polymers display negligible vapor pressure, making it difficult, if not impossible, to determine a heat of vaporization necessary to calculate the SP. Indirect assessments are thus employed. One such approximation is through internal pressure π which is viewed as a measure of the cohesive energy density. The internal pressure is then expressed as follows

$$\pi = \left(\frac{\partial U}{\partial V}\right)_T = T\left(\frac{\partial P}{\partial T}\right)_V - P = T\left(\frac{\beta}{\kappa}\right) - P \tag{14}$$

where β and κ are the isothermal compressibility and the isobaric expansivity, respectively. And, thus, the SP is expressed as follows [32]:

$$\sigma = \left(\frac{\Delta U}{V}\right)^{1/2} \approx \left(\frac{\partial U}{\partial V}\right)^{1/2} = \pi^{1/2} \tag{15}$$

The isothermal compressibility and isobaric expansivity are expressed with SL EoS using following equations [26]:

$$\kappa = -\frac{1}{V}\left(\frac{\partial V}{\partial P}\right)_T = \frac{1}{\rho}\left(\frac{\partial \rho}{\partial P}\right)_T = \frac{\tilde{P}\tilde{V}^2}{P\left[\tilde{T}\tilde{V}\left(\frac{1}{\tilde{V}-1} - \frac{1}{r}\right) - 2\right]} \tag{16}$$

$$\beta = \frac{1}{V}\left(\frac{\partial V}{\partial T}\right)_P = -\frac{1}{\rho}\left(\frac{\partial \rho}{\partial T}\right)_P = \frac{1+\tilde{P}\tilde{V}^2}{T\left[\tilde{T}\tilde{V}\left(\frac{1}{\tilde{V}-1} - \frac{1}{r}\right) - 2\right]} \tag{17}$$

Finally, the SP is expressed using the SL EoS, as follows

$$\sigma = \left(\frac{\rho}{\rho^*}\right)\left(P^*\right)^{1/2} \tag{18}$$

The internal pressure does not strictly represent the cohesive energy density but represents the volume-dependent cohesion parameter, and does not account for special interactions such as hydrogen bonding [33, 34]. Therefore, the internal pressure-based SP assessments should be viewed as a low estimate of the SP.

3. Results and Discussion

3.1. Experimental data

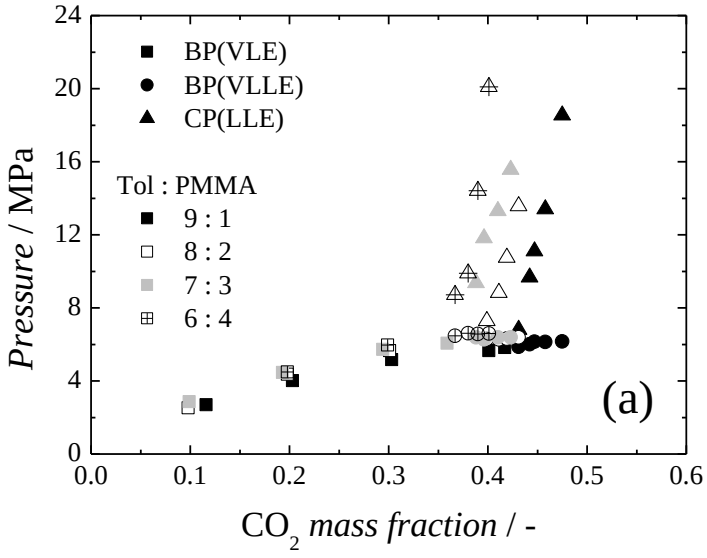

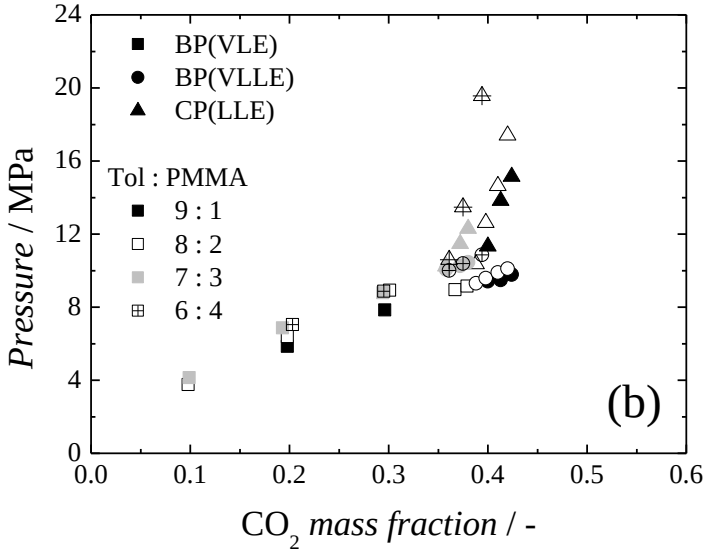

Fig. 1. Phase behavior of CO_2/Tol/PMMA ternary system ((a) 313.15 K and (b) 353.15 K).

The experimental results are shown in Figures 1, 2, 6, and 8. Figure 1 is the typical phase diagram of the CO_2/Tol/PMMA ternary system. When the CO_2 mass fraction was low, the BP, at which the VL phase separation occurs, was observed in the initially homogeneous mixture. On the other hand, when the CO_2 mass fraction was high, the CP, at which the LL

phase separation occurs, was observed. Further decrease in pressure led to the formation of the vapor phase at the VLL phase separation (also defined as BP). The phase behaviors of the CO_2/Tol/PMMA ternary system were classified into two types. These behaviors are similar to those the CO_2/Tol/PS and CO_2/silicon alkoxide/polymer ternary systems [18-20], which have been described in detail previously [18].

3.2. Comparison with the binary system

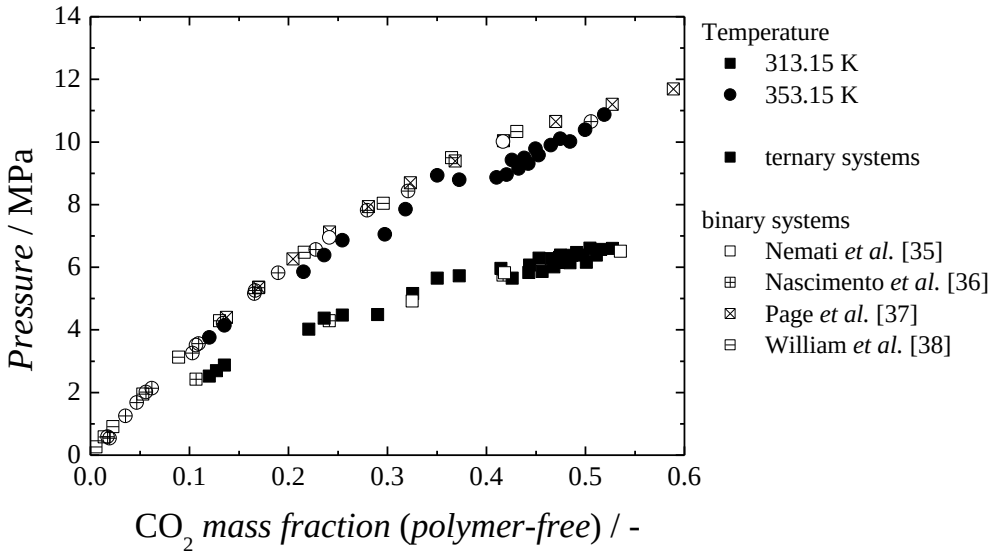

Fig. 2. Comparison between CO_2/Tol/PMMA ternary and CO_2/Tol binary systems [35-38].

In Figure 2, the VL and VLL points of the CO_2/Tol/PMMA ternary system are shown with polymer-free bases. The VL points of a CO_2/Tol binary system are also shown in the figure. As can be seen from the figure, the VL points of the binary system are almost identical to the VL and VLL lines of the CO_2/Tol/PMMA systems. Based on this comparison, it could be deduced that the polymer is not involved in the separation of the vapor phase from the homogeneous mixture.

3.3. Estimation of Free volume and Solubility parameter

Figure 3(a) shows the FV of pure components estimated using SL EoS. As can be seen from the figure, the FV was Tol<CO_2<PS<PMMA in decreasing order except at extremely low pressure. The FV of CO_2 changed greatly depending on the phase state. The FV of gaseous CO_2

varied greatly with pressure, and was larger than that of polymers at extremely low pressure. On the other hand, the change in FV as a function of pressure became smaller in the liquid state and supercritical state, and the FV was almost the same as that of Tol. The FV of all substances decreased with increasing pressure and increased with increasing temperature. Figure 3(b) shows the FV of the CO_2/Tol homogeneous mixture estimated using SL EoS. It can be seen from the figure that the FV of the mixture decreases with the increase in pressure and decreases with the increase in temperature. Figure 3(c) shows CO_2 composition dependence of the FV of the CO_2/Tol homogeneous mixture. It can be seen from the figures that the FV of the mixture is not the average value of each component, and changes with the mixing. Although the FV changed with composition, the amount of change was much smaller than the difference in FV due to polymer species in Figure 3(a).

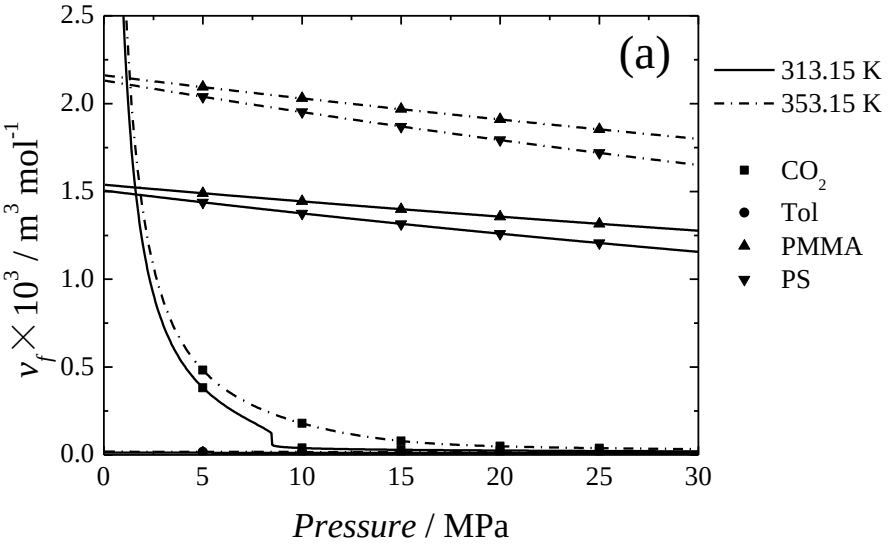

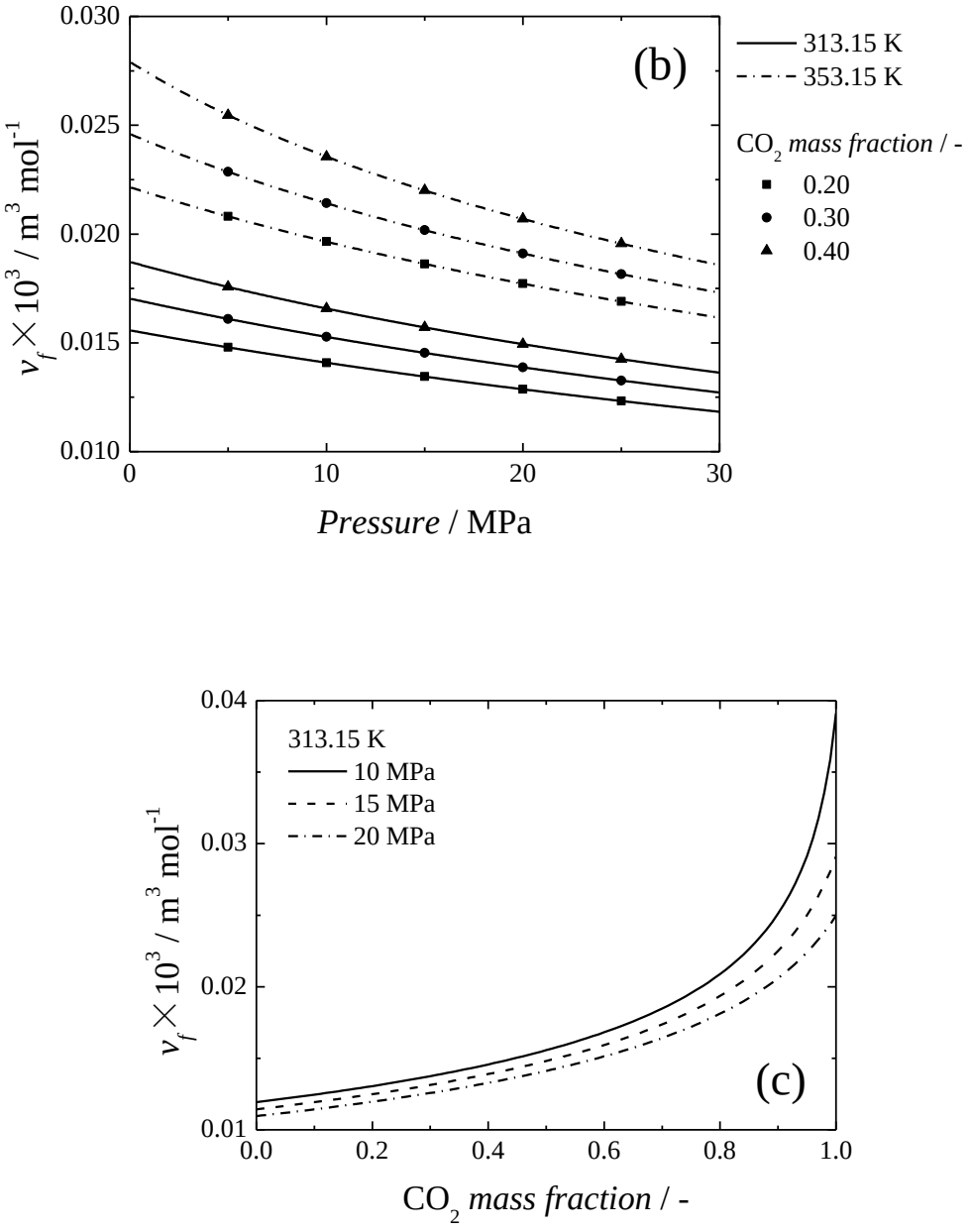

Fig. 3. Estimation results of free volume ((a) pure components, (b) and (c) homogeneous mixture of CO_2/Tol).

Figure 4(a) shows the SPs of pure components estimated using SL EoS. As can be seen from the figure, the SPs are CO_2<Tol<PS<PMMA in descending order. The SP of CO_2 changed significantly according to the change in phase state. Due to their similarity in molecular structures, the SPs of Tol and PS showed very similar values. The SPs of all substances increased with the increase in pressure and decreased with the increase in temperature. Figure 4(b) shows the estimation results of the SP of the CO_2/Tol homogeneous mixture using SL EoS.

It can be seen from the figure that the solubility parameter of CO_2/Tol mixture not only depends on the pressure and temperature similar to pure components, but also depends on the CO_2 composition. Figure 4(c) shows the CO_2 composition dependence of the SP of CO_2/Tol mixture. Similar to the FV, the SP of the mixture is not the average value of individual pure components, and changes with the mixing.

The difference in FV ($\Delta v_f = v_{f,polymer} - v_{f,CO_2+Tol}$) and SP ($\Delta\sigma = \sigma_{polymer} - \sigma_{CO_2+Tol}$) between components is an indicator of compatibility and affinity. In general, the smaller the difference in FV and SPs, the better the compatibility and affinity between the components.

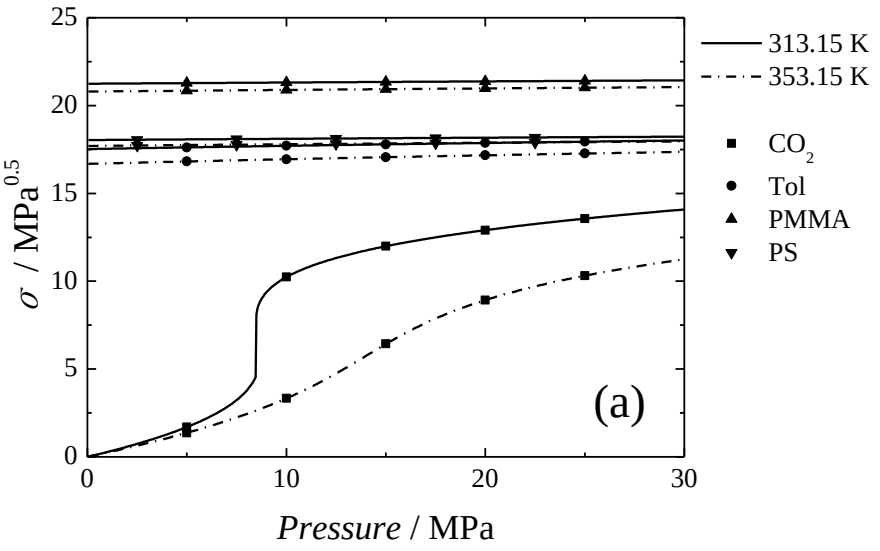

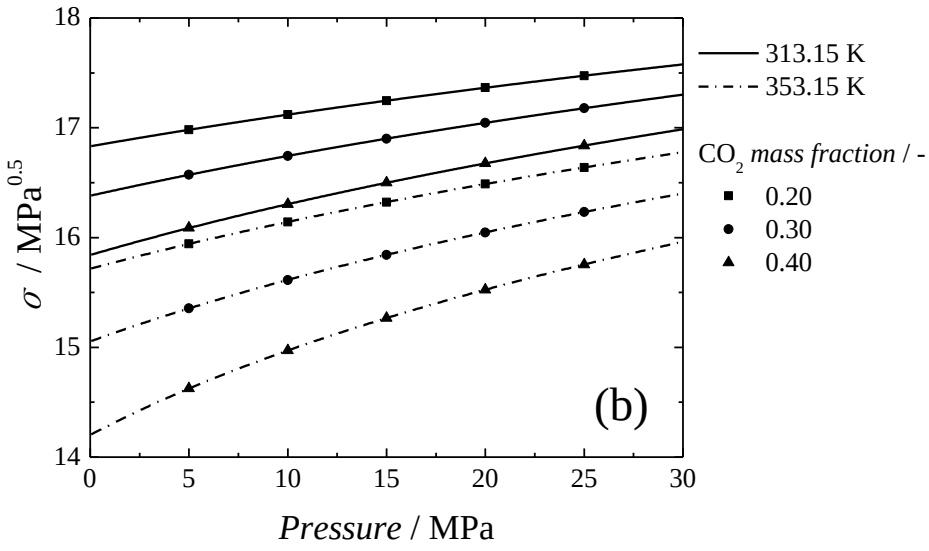

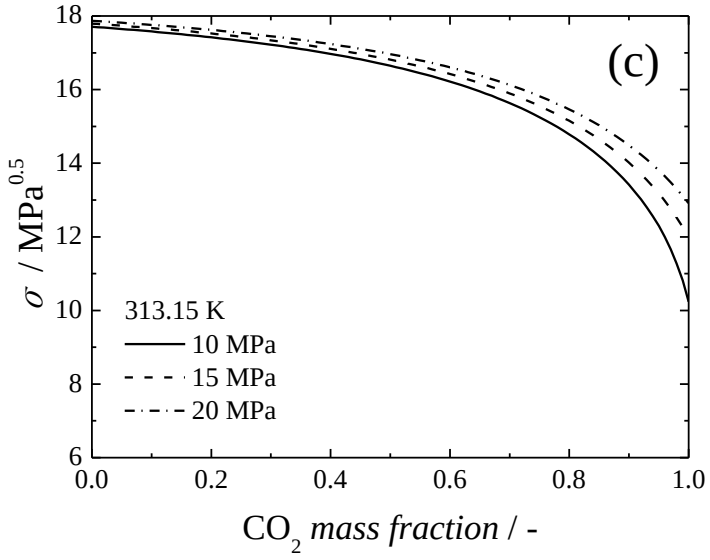

Fig. 4. Estimation results of solubility parameter ((a) pure component, (b) and (c) homogeneous mixture of CO_2/Tol).

3.4. Effect of Polymer concentration

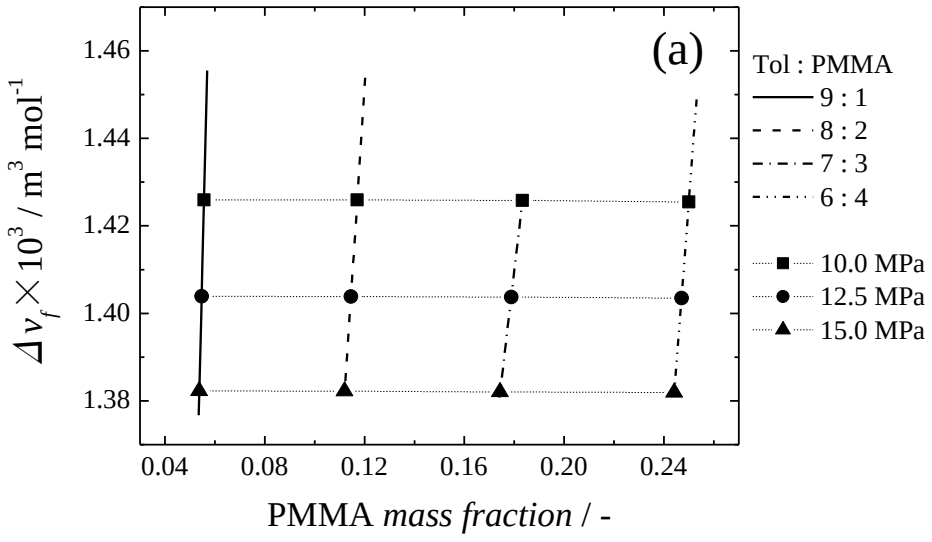

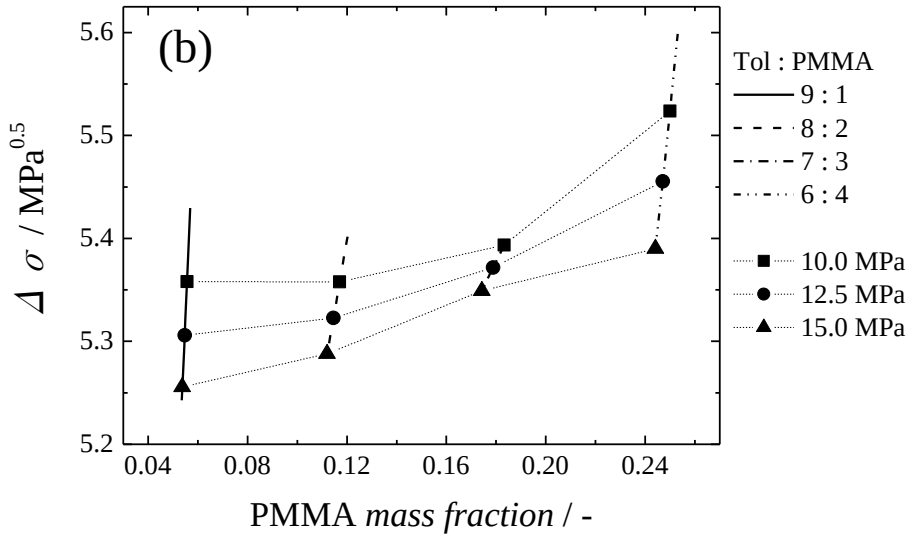

Fig. 5. Effects of polymer concentration on the difference in (a) free volume and (b) solubility parameter on the CP.

Figure 1 shows the effect of the ratio of the Tol and PS on the CO_2/Tol/PMMA ternary system. As ratio of PMMA increased, the VLL and VL lines shifted to a higher pressure and the LL lines shifted to a lower CO_2 mass fraction. Figure 5(a) and (b) show the effect of polymer concentration on the difference in FV and SPs between PMMA and CO_2/Tol mixtures on the CP, respectively. CP in the figure is the interpolated value of the phase diagram. The differences in FV and SPs in the compositions of the CPs determined by interpolation were calculated. Liquid-liquid phase separation occurred when the FV or SP difference shown in the figure was exceeded. Figure 5(a) shows that the FV difference decreased as the CP shifted to higher pressure. Furthermore, at the same CP pressure, the FV difference was almost constant regardless of the polymer concentration. It can be read that under the same pressure, phase separation occurs when the FV difference exceeds a certain value. On the other hand, Figure 5(b) shows that the difference in SPs increases as the CP shifted to lower pressure and with increasing polymer concentration at the same CP pressure. Under the same CP pressure, the larger the polymer concentration, the lower the CO_2 composition and the phase separation. There was a possible correlation between the change in the SP difference and the decrease in the homogeneous phase region.

3.5. Effect of Temperature

Figure 6 shows the effect of the temperature on the CO_2/Tol/PMMA ternary system.

As seen in the figure, upon increasing of the temperature, the VL and VLL lines shifted to higher pressures, analogous to the behavior of the CO_2/Tol binary system. On the other hand, the LL line shifted to lower CO_2 compositions. Figures 7(a) and (b) show the effect of temperature on the difference in FV and SPs of PMMA and CO_2/Tol mixture on the CP, respectively. CP in the figure is the interpolated value of the phase diagram. The differences in FV and SPs in the compositions of the CPs determined by interpolation were calculated. From the figure, the difference in FV and SPs increased as the temperature increased from 313 K to 353 K. This means that the compatibility decreased as well as the effect of polymer concentration. In the phase diagram, the homogeneous phase region became smaller as the temperature increased. This could be correlated with the change in FV and SP difference.

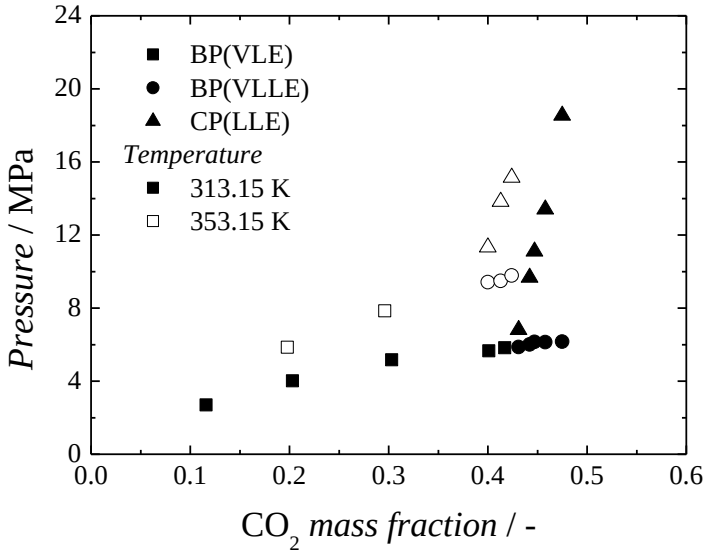

Fig. 6. Effects of temperature on the phase behavior of CO_2/Tol/PMMA ternary systems (Tol : PMMA = 9 : 1).

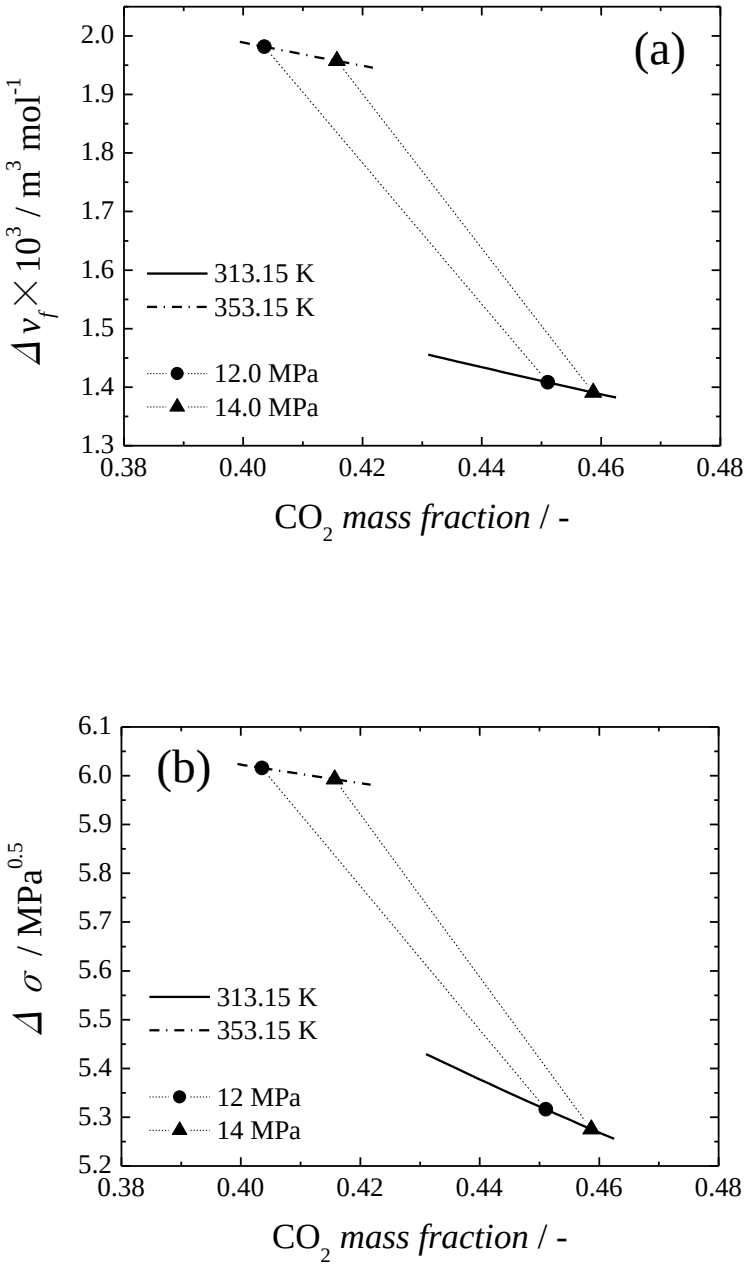

Fig. 7. Effects of temperature on the difference in (a) free volume and (b) solubility parameter on the CP.

3.6. Effect of Polymer species

Figure 8 also shows the experimental results of the CO_2/Tol/PS ternary system reported in previous work [20]. In the *Px* phase diagram of the ternary system, the VLL and VL lines for both polymers are identical. These facts are discussed in detail in Section 3.2. On the other hand,

the LL line of PS separates from the VL line at a lower CO_2 mass fraction compared to PMMA, and it shows greater CO_2 mass fraction dependence. Figure 9(a) and (b) show the effect of polymer species on the difference in FV and SPs between polymer and CO_2/Tol mixtures on the CP, respectively. The figure shows that the difference in FV and SPs of PS is smaller than that of PMMA. It is known that the carbonyl group of PMMA and CO_2 have a specific interaction like a Lewis acid base. It was reported that the solubility of CO_2 is larger in PMMA than in PS. Based on the above facts, PMMA has a better affinity for CO_2 than PS. The free volume is just the volume of voids in each substance, and does not consider the interactions between components. On the other hand, as mentioned in Section 2.3.3, the solubility parameter estimated in this study is based on internal pressure and does not consider interactions such as hydrogen bonding. Therefore, it should be considered that the solubility parameter is a low estimate. These led to discrepancies between the differences in free volume and solubility parameters and the trends of the homogeneous phase region in the phase diagram.

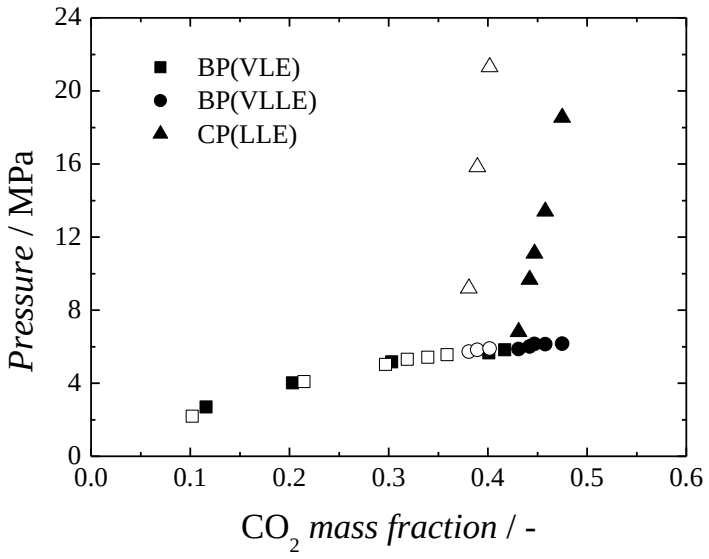

Fig. 8. Effects of polymer species on the phase behavior of CO_2/Tol/Polymer ternary systems (313.15 K, Tol : Polymer = 9 : 1, closed symbols PMMA, open symbols PS).

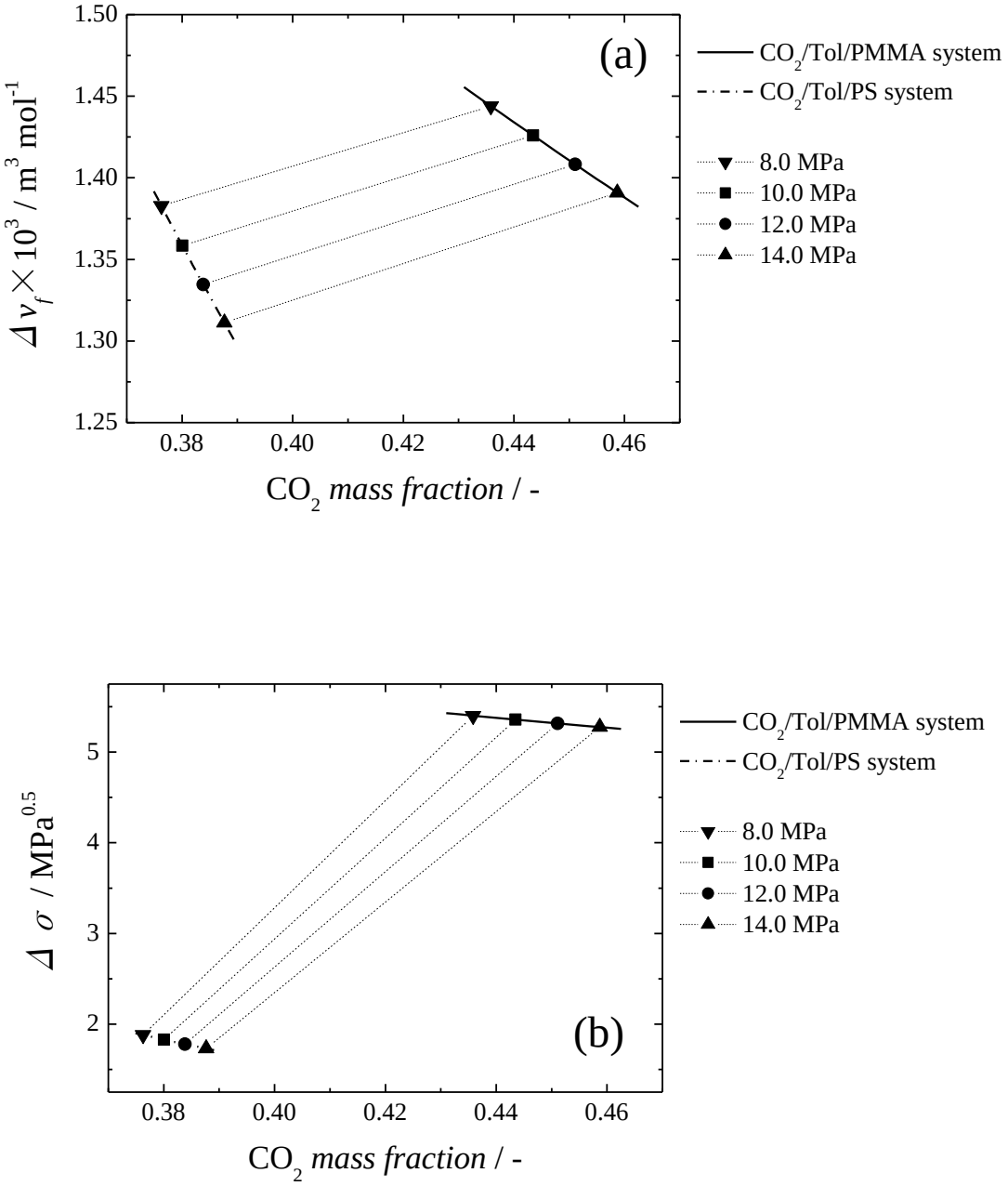

Fig. 9. Effects of polymer species on the difference in (a) free volume and (b) solubility parameter on the CP.

4. Conclusions

A phase diagram for the CO_2/Tol/PMMA ternary system was obtained over a wide range of temperatures, pressures, and polymer mass fractions. The LL line of PS separates from the VL line at a lower CO_2 mass fraction compared to PMMA, and it shows greater CO_2 mass

fraction dependence. Furthermore, the LL lines shifted to a lower CO_2 mass fraction as ratio of PMMA increased or/and temperature decreased. The free volume and solubility parameters of each component and CO_2/Tol mixture were estimated using the SL EoS. By estimating the difference in free volume and solubility parameters between the polymer and CO_2/Tol mixture, it was explained that the effect of polymer concentration and temperature on LLE. On the other hand, the solubility parameters estimated in this study do not consider interactions such as hydrogen bonding and are low estimates, so they could not explain the difference in LLE between PMMA and PS. These results are important for understanding the phase behaviors of CO_2/organic solvent/polymer systems. In this study, we discussed the effect of polymer species, and in the future, the effect of co-solvent organic solvent species will be discussed to deepen our understanding of the phase behavior of the CO_2/organic solvent/polymer system.

References

[1] J.M. DeSimone, E.E. Maury, Y.Z. Menceloglu, J.B. McClain, T.J. Romack, J.R. Combes, Dispersion Polymerizations in Supercritical Carbon Dioxide, Science, 265 (1994) 356-359.

[2] D.A. Canelas, D.E. Betts, J.M. DeSimone, Dispersion Polymerization of Styrene in Supercritical Carbon Dioxide: Importance of Effective Surfactants, Macromolecules, 29 (1996) 2818-2821.

[3] S.P. Bassett, A.D. Russell, P. McKeown, I. Robinson, T.R. Forder, V. Taresco, M.G. Davidson, S.M. Howdle, Low-temperature and purification-free stereocontrolled ring-opening polymerisation of lactide in supercritical carbon dioxide, Green Chemistry, 22 (2020) 2197-2202.

[4] D.J. Dixon, K.P. Johnston, R.A. Bodmeier, Polymeric Materials Formed by Precipitation with a Compressed Fluid Antisolvent, AIChE Journal, 39 (1993) 127-139.

[5] V. Prosapio, E. Reverchon, I. De Marco, Polymers' ultrafine particles for drug delivery systems precipitated by supercritical carbon dioxide + organic solvent mixtures, Powder Technology, 292 (2016) 140-148.

[6] P. Franco, E. Reverchon, I. De Marco, PVP/ketoprofen coprecipitation using supercritical antisolvent process, Powder Technology, 340 (2018) 1-7.

[7] A. Salerno, C. Domingo, Polycaprolactone foams prepared by supercritical CO_2 batch foaming of polymer/organic solvent solutions, The Journal of Supercritical Fluids, 143 (2019) 146-156.

[8] C.F. Kirby, M.A. McHugh, Phase Behavior of Polymers in Supercritical Fluid Solvents, Chemical Reviews, 99 (1999) 565-600.

[9] H.-Y. Lee, S.-D. Yoon, H.-S. Byun, Cloud-Point and Vapor-Liquid Behavior of Binary and Ternary Systems for the Poly(dodecyl acrylate) + Cosolvent and Dodecyl Acrylate in Supercritical Solvents, J. Chem. Eng. Data, 55 (2010) 3684-3689.

[10] C.-R. Kim, H.-S. Byun, Effect of cosolvent on the phase behavior of binary and ternary mixture for the poly(2-dimethylaminoethyl methacrylate) in supercritical solvents, Fluid Phase Equilibria, 381 (2014) 51-59.

[11] D.-S. Yang, S.-H. Cho, S.-D. Yoon, H.-H. Jeong, H.-S. Byun, Phase behavior measurement for poly(isobornyl acrylate)+cosolvent systems in supercritical solvents at high pressure, The Journal of Supercritical Fluids, 79 (2013) 11-18.
[12] H.-S. Byun, Co-solvent concentration influence of two- and three-component systems on the high pressure cloud-point behavior for the poly(vinyl stearate) under supercritical CO_2, Journal of Industrial and Engineering Chemistry, 90 (2020) 76-84.
[13] B.M. Hasch, M.A. Meilchen, S.-H. Lee, M.A. McHugh, Cosolvency effects on copolymer solutions at high pressure, Journal of Polymer Science Part B: Polymer Physics, 31 (1993) 429-439.
[14] R. Campardelli, E. Reverchon, I. De Marco, PVP microparticles precipitation from acetone-ethanol mixtures using SAS process: Effect of phase behavior, The Journal of Supercritical Fluids, 143 (2019) 321-329.
[15] T.M.M. Santos, E.A. Rebelatto, B.B. Chaves, M. Lanza, J.V. Oliveira, E.C.M.C. Albuquerque, S.A.B. Vieira de Melo, High pressure phase equilibrium data for carbon dioxide, methyl methacrylate and poly (dimethylsiloxane) systems, The Journal of Supercritical Fluids, 143 (2019) 346-352.
[16] B. Kim, J. Gwon, T. Im, H.Y. Shin, H. Kim, High-Pressure Phase Behavior of Poly(lactic-co-glycolic acid), Dichloromethane, and Carbon Dioxide Ternary Mixture Systems, Journal of Chemical & Engineering Data, 60 (2015) 2146-2151.
[17] J. Gwon, S.H. Kim, H.Y. Shin, H. Kim, Phase Behavior of Poly(d-lactic acid), Dichloromethane, and Carbon Dioxide Ternary Mixture Systems at High Pressure, Journal of Chemical & Engineering Data, 59 (2014) 2144-2149.
[18] H. Matsukawa, Y. Shimada, S. Yoda, Y. Okawa, M. Naya, A. Shono, K. Otake, Phase behavior of Carbon dioxide/Tetramethyl orthosilicate/polymer ternary systems, Fluid Phase Equilibria, 457 (2018) 1-10.
[19] H. Matsukawa, S. Yoda, Y. Okawa, K. Otake, Phase Behavior of a Carbon Dioxide/Methyl Trimethoxy Silane/Polystyrene Ternary System, Polymers (Basel), 11 (2019).
[20] H. Matsukawa, M. Otsuka, K. Otake, Phase-equilibrium measurement of a carbon dioxide/toluene/polystyrene ternary system using laser turbidimetry, Fluid Phase Equilibria, 509 (2020) 112464.
[21] J.S. Dickmann, J.C. Hassler, E. Kiran, Modeling of the volumetric properties and estimation of the solubility parameters of ionic liquid+ethanol mixtures with the Sanchez–Lacombe and Simha–Somcynsky equations of state: [EMIM]Ac+ethanol and [EMIM]Cl+ethanol mixtures, The Journal of Supercritical Fluids, 98 (2015) 86-101.
[22] M.L. Williams, J.S. Dickmann, J.C. Hassler, E. Kiran, Volumetric Properties and Solubility Parameters of Cyclohexane + CO_2 Mixtures at High Pressures and Their Modeling with the Sanchez–Lacombe Equation of State, Industrial & Engineering Chemistry Research, 56 (2017) 8748-8766.

[23] M.E. McCorkill, J.S. Dickmann, E. Kiran, Effect of Alkyl Chain Length on Derived Thermodynamic Properties of 1-Alkyl-3-methylimidizolium Chloride Ionic Liquids and Their Mixtures with Ethanol, Industrial & Engineering Chemistry Research, 58 (2019) 15649-15665.
[24] F.A.M.M. Gonçalves, C.S.M.F. Costa, C.E. Ferreira, J.C.S. Bernardo, I. Johnson, I.M.A. Fonseca, A.G.M. Ferreira, Pressure–volume–temperature measurements of phosphonium-based ionic liquids and analysis with simple equations of state, The Journal of Chemical Thermodynamics, 43 (2011) 914-929.
[25] R.H. Lacombe, I.C. Sanchez, Statistical Thermodynamics of Fluid Mixtures, J. Phys. Chem., 80 (1976) 2568-2580.
[26] I.C. Sanchez, R.H. Lacombe, An Elementary Molecular Theory of Classical Fluids. Pure Fluids, J. Phys. Chem., 80 (1976) 2352-2362.
[27] I.C. Sanchez, R.H. Lacombe, Statical Thermodynamics of Polymer Solutions, Macromolecules, 11 (1978) 1145-1156.
[28] H. Matsukawa, K. Otake, Phase behavior of carbon dioxide/tetrapropyl orthosilicate and tetrabutyl orthosilicate systems, Fluid Phase Equilibria, 548 (2021) 113172.
[29] H. Matsukawa, T. Tsuji, K. Otake, Measurementof the Density of Carbon Dioxide/Toluene Homogeneous Mixtures and Correlation with Equations of State, J. Chem. Thermodynamics, (Under article submission).
[30] Y. Xiong, E. Kiran, Prediction of high-pressure phase behaviour in polyethylene/n-pentane/carbon dioxide ternary system with the Sanchez-Lacombe model, Polymer, 35 (1994) 4408-4415.
[31] S.H. Lee, S.B. Lee, The Hildebrand solubility parameters, cohesive energy densities and internal energies of 1-alkyl-3-methylimidazolium-based room temperature ionic liquids, Chem Commun (Camb), (2005) 3469-3471.
[32] J.A.R. Renunclo, G.J.F. Breedveld, J.M. Prausnltz, Internal Pressures and Solubility Parameters for Carbon Disulfide, Benzene, and Cyclohexane, The Journal of Physical Chemistry, 81 (1977) 324-327.
[33] S. Verdier, S.I. Andersen, Internal pressure and solubility parameter as a function of pressure, Fluid Phase Equilibria, 231 (2005) 125-137.
[34] V.N. Kartsev, K.E. Pankin, D.V. Batov, ON INTERRELATION BETWEEN THE INTERNAL PRESSURE AND THE COHESION ENERGY DENSITY, Journal of Structual Chemistry, 47 (2006) 277-284.
[35] E.N. Lay, Measurement and Correlation of Bubble Point Pressure in (CO_2 + C_6H_6), (CO_2 + $CH_3C_6H_5$), (CO_2 + C_6H_{14}), and (CO_2 + C_7H_{16}) at Temperatures from (293.15 to 313.15) K, J. Chem. Eng. Data, 55 (2010) 223-227.
[36] S.H. Page, S.R. Sumpter, M.L. Lee, Fluid Phase Equilibria in Supercrtical Fluid Chromatography with CO_2-Based Mixed Mobile Phases: A Review, J. Microcol. Sep., 4 (1992) 91-

122.
[37] W.O. Morris, M.D. Donohue, Vapor-liquid equilibria in mixtures containing carbon dioxide, toluene, and 1-methylnaphthalene, Journal of Chemical & Engineering Data, 30 (1985) 259-263.
[38] F.P. Nascimento, M.L.L. Paredes, A.P.D. Bernardes, F.L.P. Pessoa, Phase behavior of CO2/toluene, CO2/n-decane and CO2/toluene/n-decane: Experimental measurements and thermodynamic modeling with SAFT-VR Mie equation of state, The Journal of Supercritical Fluids, 154 (2019) 104634.